Theoret. Chim. Acta (Berl.) 43, 45–62 (1976)

THEORETICA CHIMICA ACTA


# On the Lattice Stability of Metals

## III. A Comparison of the Stability of Body-Centred and Face-Centred Cubic NFE-Metals in a Model Tight-Binding Calculation

Bernhard Reiser

*Max-Planck-Institut für Festkörperforschung, Büsnauerstraße 171, D-7000 Stuttgart 80, Federal Republic of Germany*

A tight-binding calculation for body-centred cubic (bcc) and face-centred cubic (fcc) lithium is carried out using muffin-tin potentials which differ only in the arrangement of the muffin-tin spheres. The essential results are not restricted to lithium but also hold for other metals with similar *s–p*-bands. The bcc structure can be stable for the lowest valence states. The stability of fcc increases with increasing valence electron concentration. This is due to the kinetic energy which behaves as in an empty lattice case. In accordance with the behaviour of the kinetic energy, the lowest energy states have the highest distribution probability between neighbouring atoms. They are mostly delocalized. The trend in the lattice stability is explained in terms of the differences in the packing of the lattices. In real cases where the virial theorem holds an appropriate part of the kinetic energy is changed into potential energy. Hybridization plays a completely different role from that in covalent compounds. It stabilizes a compound by delocalizing the charge density.

**Key words:** Metals - Lattice stability

### 1. Introduction

Chaney, Tung, Lafon and Lin [1-3] performed tight-binding (TB) calculations with considerable accuracy. In the present work it is shown that it is possible to compare different structures by this method. It is accomplished by changing only the arrangement of the potential spheres in a constant muffin-tin plane. Such a simple rearrangement of the atoms ensures that the effects obtained are as purely geometrical as possible and that the connection between structure on the one hand and energy, distribution probability, and localized orbitals on the other hand is as simple as possible. The TB-method in a very simple way provides analytic functions with which these structural effects can be described. This can be done specifically in terms of localized orbitals with a given point group symmetry which, for example, can be compared with the atomic orbitals. In this calculation the same set of eleven independent basis functions was sufficient to calculate the entire valence band and about half of the *p*-bands with reasonable accuracy. This allows one to reasonably speak of hybridization in a metal as mixing of localized

*s*- and *p*-basis orbitals and to discuss its role in the metallic bond. Thus the TB-method is a good means of throwing light into the black box of secular procedures in order to clarify what happens to the energy values, eigenfunctions and orbitals as a function of symmetry and range of interaction with neighbouring atoms. We will see for example that in agreement with classical chemical ideas (Krebs [4]) the lattice stability behaves, to a certain extent, as if the energy contributions from the more distant neighbours would cancel and as if it would be determined only by nearest neighbour interaction.

The pseudopotential approach is more efficient for the calculation of energy eigenvalues of a particular NFE-metal or a given NFE-alloy. But whereas the simplicity of this approach depends on keeping the formalism in *k*-space the TB-method handles the problems in **r**-space and thus can give a complementary picture of the metallic bond in the NFE-metals. Furthermore it does not depend on the existence of a repulsion potential.

A considerable difficulty in understanding the metallic bond is the very different mathematical treatment of *s*-*p*-bands by second-order pseudopotential perturbation theory (see, for example, Harrison [5] and Hafner [6–8] and Heine and Weaire [9]) and that of the *d*-bands by the resonance theory (e.g. Hubbard [10, 11], Dalton [11, 12], Deegan [13], Pettifor [14, 15]). In contrast to both these methods, the TB treatment is completely general and provides a means for treating the *d*-metals in the same way as the NFE-metals.

In the last few years it has become more and more possible to do self-consistent calculations with considerable accuracy. One may compare, for example, the work of Averill [16] or Rudge [17] or Ellis and Painter [18]. Since the work of Chaney, Lafon and Lin [19] it is also possible to do tight-binding calculations self-consistently. But besides pseudopotential calculations for NFE-metals there are only a few which compare different structures. The calculations of Kumar, Monkhurst and Harris [20] for lithium and those of Averill [21] for cesium may serve as examples.

It would also be very interesting to carry out all discussions of this work for self-consistent calculations. But this could not replace the given treatment because self-consistency would change the shape of the atomic potentials in dependence on the lattice and on the valence electron concentration. So the change of the atomic potential would influence the bonding and stability of the metals besides the lattice differences in the geometrical arrangement of the atomic potentials. We could not distinguish between both effects.

In Sect. 2 details of the method and the results are given. Section 3 gives a comparison of the results for the bcc and fcc lattices. In Sect. 4 we show that the differences in the packing of the lattices determine the differences in the energy values. In Sect. 5 we discuss the role of the potential in a metal as far as it can be treated by a non-self-consistent muffin-tin potential. Section 6 gives the connection with the virial theorem. Section 7 shows that hybridization plays a completely different role than in covalent compounds. Finally, Sect. 8 gives a glance at the transition metals, because of the generality of the TB treatment, and in Sect. 9 we summarize.

## 2. The Tight-Binding Method and its Results

The TB-method used is that of Chaney, Tung and Lafon [2]. There are only two differences:

a) The basis orbitals are constructed from pure Gaussian orbitals. This means that the $p$-type groups are represented by two Gaussian functions with unequal centre.
b) The atomic potential used in $r$-space to calculate the integrals with the strongly localized Gaussians is the polynomial form of the Seitz potential [22] given in Ref. [1] which was used to calculate the Fourier components of the potential. This makes the calculation of the potential energy completely consistent.

Each $s$-type group of Gaussians consists of a single Gaussian function the exponent of which is taken from Whitten [23]. Each $p$-type group consists of a pair of Gaussians the exponents of which have at first been taken from a lithium free atom $2p$ orbital. This orbital was obtained by a least square fitting to the one given by Fock and Petrashen [24] and is shown in Table 1. But then the exponents of these orbitals and the $t_n$ of

Table 1. Free atom $2p$ lithium orbital after Fock and Petrashen [24]

| $c_n$ | $\eta_n$ | $t_n$ | | |
|---|---|---|---|---|
| 0.0845 | 4.9862 | 0.05 | 0.0 | 0.0 |
| −0.0845 | 4.9862 | −0.05 | 0.0 | 0.0 |
| 1.4078 | 0.3848 | 0.03 | 0.0 | 0.0 |
| −1.4078 | 0.3848 | −0.03 | 0.0 | 0.0 |
| 0.3801 | 0.04805 | 0.43 | 0.0 | 0.0 |
| −0.3801 | 0.04805 | −0.43 | 0.0 | 0.0 |
| 0.0068 | 0.0083 | 1.59 | 0.0 | 0.0 |
| −0.0068 | 0.0083 | −1.59 | 0.0 | 0.0 |

Table 2. Coefficients $c_n$, exponents $\eta_n$, and centres $t_n$ of groups of Gaussians $g(\mathfrak{r}) = \Sigma_n c_n \exp(-\eta_n(\mathfrak{r} - t_n)^2)$

| $c_n$ | $\eta_n$ | $t_n/a_0^{bcc}$ | | |
|---|---|---|---|---|
| 1.0 | 34.7874 | 0.0 | 0.0 | 0.0 |
| 1.0 | 9.1187 | 0.0 | 0.0 | 0.0 |
| 1.0 | 3.7460 | 0.0 | 0.0 | 0.0 |
| 1.0 | 1.5384 | 0.0 | 0.0 | 0.0 |
| 1.0 | 0.7968 | 0.0 | 0.0 | 0.0 |
| 1.0 | 0.5507 | 0.0 | 0.0 | 0.0 |
| 1.0 | 0.1300 | 0.0 | 0.0 | 0.0 |
| 1.0 | 4.9862 | 0.015341 | 0.0 | 0.0 |
| −1.0 | 4.9862 | −0.015341 | 0.0 | 0.0 |
| 1.0 | 0.3848 | 0.009205 | 0.0 | 0.0 |
| −1.0 | 0.3848 | −0.009205 | 0.0 | 0.0 |
| 1.0 | 0.1500 | 0.032000 | 0.0 | 0.0 |
| −1.0 | 0.1500 | −0.032000 | 0.0 | 0.0 |
| 1.0 | 0.1000 | 0.131936 | 0.0 | 0.0 |
| −1.0 | 0.1000 | −0.131936 | 0.0 | 0.0 |

that group with the smallest $\eta_n$ have been varied to achieve minimal energy values in the whole band region. The exponents $\eta_n$ and the centres $\mathfrak{t}_n$ of the Gaussians of these groups $g_n$ are listed in Table 2. The groups of Gaussians have been normalized. They have been used equally in both bcc and fcc calculations.

To make the calculations as equivalent as possible, the Fourier components of the potential have been included in both lattices up to a distance of 7.7 a.u., which means that for bcc 41 stars of the reciprocal lattice and for fcc 47 stars have been included.

For the muffin-tin plane the value

$$V_{\mathrm{MT}} = -0.6629 \text{ ryd}$$

given by W. Kohn and N. Rostoker [25] and for the radius of the muffin-tin sphere the usual value

$$r_i = 0.5 \cdot a_0^{\mathrm{bcc}} \sqrt{3}$$

$$a_0^{\mathrm{bcc}} = 3.25915 \text{ a.u.}$$

was used. $a_0^{\mathrm{bcc}}$ is the half lattice constant for bcc lithium. As already mentioned going from bcc to fcc only the arrangement of the muffin-tin spheres changed. The first ten Fourier coefficients of the potentials of the bcc and fcc lattices are given in Table 3. The values for bcc are closely related to those of Schlosser and Marcus [26].

The direct lattice sums which enter the matrix elements of the secular problem have, if necessary, been calculated up to tenth nearest neighbours.

For the eigenfunctions we made the Ansatz

$$\psi_{\nu\mathfrak{t}}(\mathfrak{w}) \equiv Q_{\mathfrak{t}}(S^{\nu}_{|\mathfrak{t}|} + iP^{\nu}_{|\mathfrak{t}|}); \qquad Q_{\mathfrak{j}} \equiv \frac{1}{\sqrt{N}} \sum_{j} e^{i\mathfrak{t}\mathfrak{j}} T_{\mathfrak{j}}$$

$$S^{\nu}_{|\mathfrak{t}|} \equiv \sum_{g^s} c^{s\nu}_{|\mathfrak{t}|} g^s(\mathfrak{w}); \qquad p^{\nu}_{|\mathfrak{t}|} \equiv \sum_{g^p} c^{p\nu}_{|\mathfrak{t}|} g^p(\mathfrak{w})$$

Table 3. The first ten Fourier coefficients of the Seitz potential for bcc and fcc lithium

| bcc | | fcc | |
|---|---|---|---|
| $\frac{a_0^{\mathrm{bcc}}}{\pi}\lvert\mathfrak{k}_{\mathrm{fcc}}\rvert$ | $-V_0(\mathfrak{k})$ [ryd] | $\frac{a_0^{\mathrm{fcc}}}{\pi}\lvert\mathfrak{k}_{\mathrm{bcc}}\rvert$ | $-V_0(\mathfrak{k})$ [ryd] |
| 0 0 0 | 1.00169 | 0 0 0 | 1.00169 |
| 1 1 0 | 0.16872 | 1 1 1 | 0.17496 |
| 2 0 0 | 0.09422 | 2 0 0 | 0.14285 |
| 1 1 2 | 0.06378 | 2 2 0 | 0.07496 |
| 2 2 0 | 0.05154 | 1 1 3 | 0.05678 |
| 3 1 0 | 0.04561 | 2 2 2 | 0.05342 |
| 2 2 2 | 0.04126 | 4 0 0 | 0.04543 |
| 3 2 1 | 0.03708 | 3 3 1 | 0.04133 |
| 4 0 0 | 0.03300 | 4 2 0 | 0.04001 |
| 3 3 0 | 0.02929 | 2 2 4 | 0.03477 |

Table 4. The calculated energy values $\epsilon_{\nu\mathfrak{k}}$ given in the second column are compared with those of other authors. The numbers in the top row are literature citations. $a_0^{\text{bcc}} = 3.25915$

| | | 2 | 26 | 27 | 28 | 29 |
|---|---|---|---|---|---|---|
| $\Gamma_1$ | −0.675 | −0.674 | −0.68345 | −0.685 | −0.686 | |
| $\Gamma_{15}$ | 0.585 | | | | 0.617 | |
| $\Gamma_1$ | 2.150 | | | | 1.879 | |
| $H_{15}$ | −0.044 | −0.039 | −0.04615 | −0.047 | −0.092 | −0.009 |
| $H_1$ | 0.515 | | | 0.50 | 0.571 | |
| $P_4$ | −0.182 | −0.175 | −0.18395 | −0.182 | −0.189 | −0.1788 |
| $P_1$ | 0.161 | | 0.16265 | 0.150 | | |
| $N_1'$ | −0.410 | −0.395 | −0.41051 | −0.411 | −0.404 | −0.4128 |
| $N_1$ | −0.145 | | −0.19454 | −0.192 | −0.176 | −0.1801 |

which makes the general eigenvalue problem real. $\nu$ is the band index, $\mathfrak{k}$ the wave vector, $s$ and $p$ characterize the symmetry of the groups of Gaussians $g$, and $Q_k$ is the projection operator on a representation of the translation group. Table 4 shows energy values at highly symmetric $k$-points and compares them with the results of other authors. The results of this calculation lie deeper than those of Chaney *et al.* [2] and the higher energy values agree well with those of Schlosser and Marcus [26]. But even if this were not the case, the comparison of the two lattices would be possible because the calculations are done in the same way and therefore the errors would cancel.

## 3. The Comparison of bcc and fcc NFE-metals

Table 5 and the Figs. 1, 2 and 3 show that the TB-method is able to provide energy values accurate enough to compare different structures even in the case of compounds with very far ranging orbitals as the NFE-metals. A quantitative estimate of the energy difference between fcc and bcc lithium gives

$$E_{bs}^{\text{fcc}} - E_{bs}^{\text{bcc}} \approx -0.0002 \text{ ryd}$$

This is in agreement with the results of Hafner [6–8]. But as the figures show this comparison can be done for bcc and fcc in a very simple way using only sixteen energy values for fcc and eighteen for bcc. We make use of two facts:

a) Going from one of the directions 100, 110 and 111 to another the $s$-band changes only little.
b) For bcc and fcc the directions 110 and 111 respectively have almost equal distances from $\Gamma_1$ to the surface of the Brillouin zone. This is shown in Figs. 1, 2 and 3.

The states of bcc lie slightly deeper (about 0.001 to 0.003 ryd) than those of fcc in a sphere with radius $a_0^{\text{lat}}/\pi \cdot k = 0.3$ and along the $\Gamma P$ line ($\Gamma K$). But the states of fcc above about $a_0^{\text{lat}}/\pi \cdot k = 0.5$ and along the directions 100 and 111 lie drastically deeper (about 0.02 to 0.06 ryd). So we may say that with increasing valence electron concentration at first bcc is stable and then, at least up to the energy at point $X$, fcc becomes stable. The effect along the direction 100 and immediately below $k_F$ is so strong that we may say that for one electron per atom not only fcc but also hcp is favoured against bcc, because the differences between hcp and fcc are much smaller than that between bcc and fcc.

Table 5. Energy values of the valence and conduction band for several $\vec{k}$-points. $A$ gives the length and 100, 110 respectively 111 the direction of $\vec{k}$

| $A$ | bcc 100 | fcc 100 | bcc 111 | fcc 110 | bcc 110 | fcc 111 |
|---|---|---|---|---|---|---|
| $\Gamma_1$ | −0.675 | −0.674 | | | | |
| $\Gamma_{15}$ | 0.585 | 0.564 | | | | |
| 0.1 | −0.668 | −0.668 | | | | |
| | 0.583 | 0.569 | | | | |
| 0.3 | −0.614 | −0.614 | −0.615 | 0.615 | −0.615 | −0.615 |
| | 0.512 | 0.545 | 0.390 | 0.375 | 0.316 | 0.243 |
| 0.45 | | | | −0.540 | −0.540 | |
| | | | | 0.263 | 0.099 | |
| $\vec{k}_F$ | −0.411 | −0.415 | −0.419 | −0.417 | −0.436 | −0.445 |
| | 0.466 | 0.206 | 0.204 | 0.170 | −0.105 | −0.165 |
| $L_1'$ | | | −0.360 | −0.357 | −0.412 | −0.429 |
| $L_1$ | | | 0.184 | 0.144 | −0.142 | −0.189 |
| $N_1'$ | | | | −0.339 | −0.410 | |
| $N_1$ | | | | 0.137 | −0.145 | |
| 0.75 | −0.285 | −0.328 | | | | |
| | 0.464 | 0.077 | | | | |
| $X$ | −0.237 | −0.320 | −0.257 | −0.254 | | |
| | 0.462 | 0.066 | 0.165 | 0.115 | | |
| $K$ | | | −0.207 | −0.204 | | |
| | | | 0.161 | 0.109 | | |
| $P_4$ | | | −0.182 | | | |
| $P_1$ | | | 0.161 | | | |
| $H_{15}$ | −0.044 | | | | | |
| $H_1$ | 0.515 | | | | | |

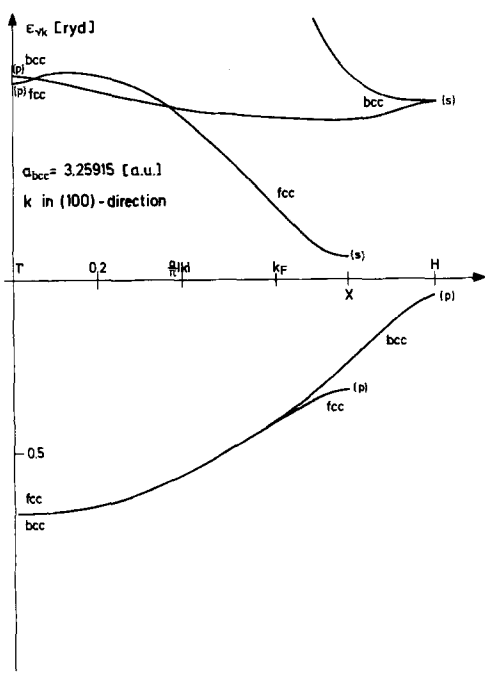


Fig. 1. $s$- and $p$-bands of lithium

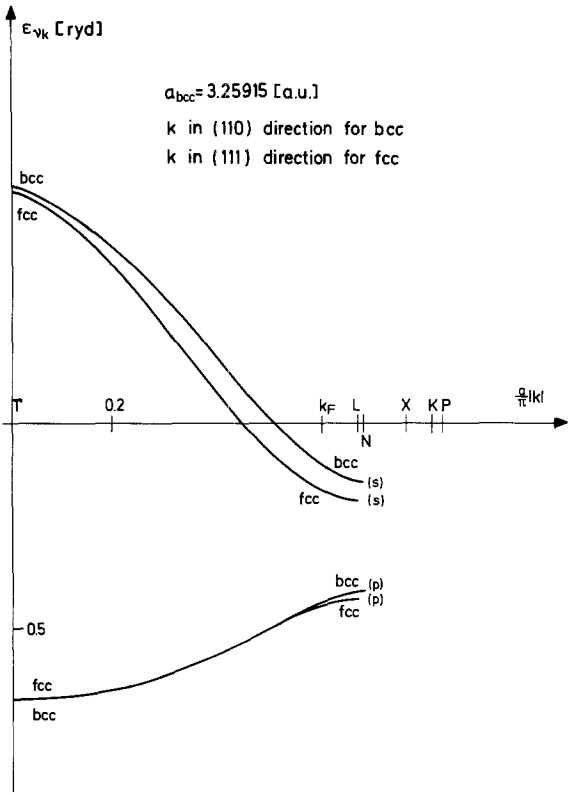


Fig. 2. *s*- and *p*-bands of lithium

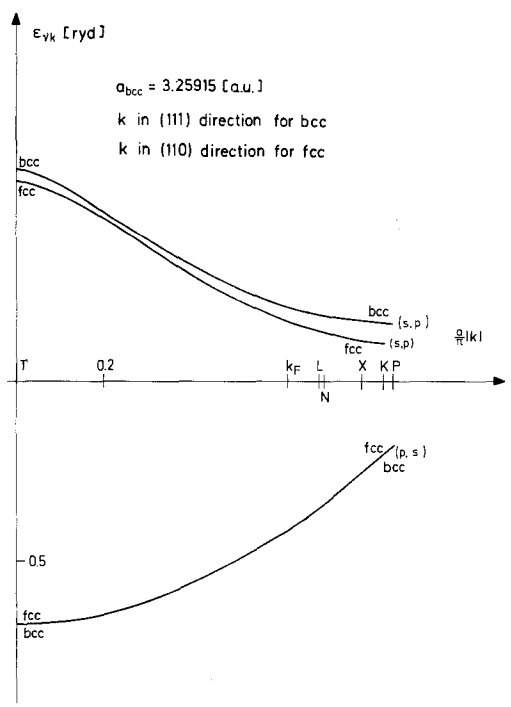


Fig. 3. *s*- and *p*-bands of lithium

Table 6. Mean values of the kinetic energy of the valence and conduction band for several $\vec{k}$-points. $A$ gives the length and 100, 110 respectively 111 the direction of $\vec{k}$

| $A$ | bcc 100 | fcc 100 | bcc 111 | fcc 110 | bcc 110 | fcc 111 |
|---|---|---|---|---|---|---|
| $\Gamma_1$ | 0.694 | 0.699 | | | | |
| $\Gamma_{15}$ | 2.014 | 1.957 | | | | |
| 0.1 | 0.693 | 0.693 | | | | |
| | 2.007 | 2.023 | | | | |
| 0.3 | 0.677 | 0.679 | 0.675 | 0.676 | 0.676 | 0.676 |
| | 2.095 | 2.175 | 1.889 | 1.791 | 1.694 | 1.513 |
| 0.45 | | | | 0.662 | 0.656 | |
| | | | | 1.776 | 1.465 | |
| $\vec{k}_F$ | 0.703 | 0.688 | 0.657 | 0.664 | 0.578 | 0.541 |
| | 2.413 | 1.766 | 2.016 | 1.815 | 1.384 | 1.313 |
| $L_1'$ | | | 0.668 | | 0.531 | 0.500 |
| $L_1$ | | | 2.078 | | 1.344 | 1.412 |
| $N_1'$ | | | | 0.679 | 0.527 | |
| $N_1$ | | | | 1.842 | 2.617 | |
| 0.75 | 0.768 | 0.663 | | | | |
| | 2.425 | 1.754 | | | | |
| $X$ | 0.803 | 0.655 | 0.710 | 0.710 | | |
| | 2.294 | 1.762 | 2.164 | 1.862 | | |
| $K$ | | | 0.747 | 0.740 | | |
| | | | 2.185 | 1.861 | | |
| $P_4$ | | | 0.771 | | | |
| $P_1$ | | | 2.189 | | | |
| $H_{15}$ | 1.027 | | | | | |
| $H_1$ | 2.927 | | | | | |

Table 6 shows the kinetic energy of the states given in Table 5. We see that the kinetic energy determines whether the energy value of bcc or fcc is lower. This behaviour is immediately connected with the distribution probability in the centre between neighbouring atoms along the directions 100, 110 and 111 as is shown in Table 7. The distribution probability at these points is a measure of its delocalization in the unit cell. A small distribution probability there means a high kinetic energy.

That these results are of a considerable generality, that they do not hold only for lithium but also for the other *s-p*-metals, is shown by an empty lattice test, the results of which are shown in Table 8. Here the same calculation as above was made with the potential equal to zero. It shows the same trends for both bands as the calculation with the Seitz potential. At first this confirms the relation between the differences in energy and the delocalization of the states we found above. Secondly it shows that only by symmetry reasons does one lattice favour the delocalization of the states (either at $\Gamma_1$ or at the band edge) and therefore the one energy more than the other. If it would be no symmetry effect, it would be an effect of the incomplete system of basis functions or one of the shape of the atomic potential. The first possibility is excluded because of the agreement of our bcc calculation with the APW [30] calculation of Schlosser and Marcus [26], especially in the region where the trend in the energy difference between bcc and fcc is

Table 7. Distribution probability $\rho_{\nu\mathfrak{k}}(\mathfrak{r})$ of the states $\psi_{\nu\mathfrak{k}}(\mathfrak{r})$ at three points $\mathfrak{r}$. $A$ gives the length of $\mathfrak{k}_A$ and 100, 110 respectively 111 its direction ($\mathfrak{r}/a_0^{\text{lat}}$) takes for the lattice (lat) the values

| bcc | fcc |
|---|---|
| 0.5 · (111) | 0.5 · (110) |
| 1.0 · (100) | 1.0 · (100) |
| 1.0 · (110) | 1.0 · (111) |

| $A$ | bcc 100 | fcc 100 | bcc 111 | fcc 110 | bcc 110 | fcc 111 |
|---|---|---|---|---|---|---|
| $\Gamma$ | 0.00850 | 0.00839 | | | | |
| | 0.00748 | 0.00609 | | | | |
| | 0.00748 | 0.00609 | | | | |
| $L$ | | | | | 0.1041 | 0.1389 |
| | | | | | 0.0844 | 0.0961 |
| | | | | | 0.0005 | 0.0961 |
| $X$ | 0.0395 | 0.0827 | | | | |
| | 0.0252 | 0.0000 | | | | |
| | 0.0690 | 0.0000 | | | | |
| $K$ | | | 0.1464 | 0.1772 | | |
| | | | 0.0503 | 0.1092 | | |
| | | | 0.0503 | 0.1092 | | |

Table 8. $\epsilon_{\nu\mathfrak{k}}$ values obtained from the Schrödinger equation with vanishing potential $V(\mathfrak{r}) = 0$ for the same set of basis orbitals as in the calculation for the Seitz potential

| $A$ | bcc 100 | fcc 100 | bcc 111 | fcc 110 | bcc 110 | fcc 111 |
|---|---|---|---|---|---|---|
| $\Gamma$ | 0.001($s$) | 0.002($s$) | | | | |
| | 1.856($p$) | 1.742($p$) | | | | |
| $L$ | | | | | 0.447($sp$) | 0.439($p$) |
| | | | | | 0.506($sp$) | 0.450($s$) |
| $X$ | 0.587($p$) | 0.585($p$) | | | | |
| | 0.988($s$) | 0.658($s$) | | | | |
| $K$ | | | 0.659($sp$) | 0.659($sp$) | | |
| | | | 0.711($sp$) | 0.688($sp$) | | |

strongest. For example at the $k$-points $X$ and $L$ our bcc-fcc differences are 0.083 and 0.017 ryd whereas the tight binding APW differences are 0.000 and 0.001 ryd respectively. The second possibility is impossible because of the empty lattice potential.

The atomic potentials can differ considerably. They are responsible for the differences of the metals, for example the differences in the valence electron concentrations where the energies of two lattices are exactly equal. So, general trends in the behaviour of the metals can only be understood by the lattice differences. But these can determine the trend in the energy differences only if the atomic potentials in the valence region are

weak enough. This condition is fulfilled so extensively for no other group of substances than the metals.

That this trend in energy differences we found is no specific property of lithium is seen also by a further argument: although often the *s*- and *p*-symmetry of the bands is not the same as for lithium, however, the relationship between the bands remain the same going from one metal to another. But as is seen from Table 5 or Figs. 1, 2, and 3 the difference between the fcc and bcc bands increases going from the *s*-band to the *p*-bands, at least up to the middle of the *p*-bands. Thus it does not depend on the symmetry of the states.

## 4. The Effect of the Geometrical Packing of the Lattices

In Table 9 we show the values of the function

$$f(\mathfrak{r}) = \sum_{j}^{s} e^{-\eta(\mathfrak{r}-j)^2}$$

for different values of $\eta$ and $s$. $\mathfrak{r}$ is the vector to the half neighbour distance in both lattices and $s$ is the number of lattice stars. The $f(\mathfrak{r})$ value for bcc, independently from $\eta$, is always larger than for fcc after convergence of the lattice sum has been achieved. This is due to the fact that bcc has smaller lattice vectors which can be seen more clearly if we define a mean length of the lattice vectors as

$$|j_s| = \sum_{j}^{s} |j| / \sum_{j}^{s} 1.0$$

The calculated results are shown in Table 10 for the three metal lattices. The $j_s$ values are smallest for bcc and those of hcp lie between bcc and fcc or are equal to that of fcc.

That this difference in the geometrical packing determines the trend of the band structure energy difference is confirmed by the discussion given in connection with the empty lattice test at the end of the last paragraph.

As for $f(\mathfrak{r})$, the packing effect causes the distribution probability of the states lowest in energy for bcc to be larger (on the surface of the unit cell, Table 7) than that for fcc. Because of the influence of the phase factor $e^{i\mathfrak{r}j}$ and the hybridization, the packing intensifies the opposite effect as the energy increases, i.e. for lower energy it favours

Table 9. Convergence values of $f(\mathfrak{r}) = \Sigma_j e^{-\eta(\mathfrak{r}-j)^2}$. $j$ are lattice vectors for the half lattice constant $a_0^{bcc} = 1.0$. $\mathfrak{r}/a_0^{lat}$ is given for the lattice lat at the top of the corresponding columns. The last column gives the number of lattice stars for which convergence is achieved

| $\eta$ | bcc 0.5(111) | fcc 0.5(110) | bcc 1.0(100) | fcc 1.0(100) | bcc 1.0(110) | fcc 1.0(111) | Star |
|---|---|---|---|---|---|---|---|
| 34.7874 | $9.33 \cdot 10^{-12}$ | $2.04 \cdot 10^{-12}$ | $1.56 \cdot 10^{-15}$ | 0.0 | $1.56 \cdot 10^{-15}$ | 0.0 | 1–2 |
| 9.1187 | 0.002142 | 0.001438 | 0.0002192 | 0.000003 | 0.0002192 | 0.000003 | 1–3 |
| 3.746 | 0.1207 | 0.1028 | 0.0495 | 0.0157 | 0.0494 | 0.0157 | 1–3 |
| 1.5384 | 0.7224 | 0.7031 | 0.6183 | 0.5273 | 0.6183 | 0.5273 | 3–4 |
| 0.7968 | 1.9572 | 1.9556 | 1.9413 | 1.9170 | 1.9413 | 1.9170 | 5–7 |
| 0.5507 | 3.406373 | 3.406288 | 3.404625 | 3.400901 | 3.404625 | 3.400901 | 9–13 |

Table 10. For the star $s$ given in the first column the contribution to $f(\mathbf{r}) \equiv \Sigma_{\mathbf{j}} e^{-\eta(\mathbf{r}-\mathbf{j})^2}$ is shown. $\mathbf{j}$ are lattice vectors to the half lattice constant $a_0^{bcc} = 1.0$. $\overline{j_s}$ are the mean distances for the three lattices bcc, fcc and hcp defined by $\overline{j_s} \equiv \Sigma_1^s |\mathbf{j}| / \Sigma_1^s$ 1.0. $\overline{j_s}$ of fcc and hcp are compared for equal distances $|\mathbf{j}|$. For bcc and fcc we may make the comparison in the given way up to a star where for both lattices the convergence of $f(\mathbf{r})$ has been achieved. $\eta = 0.5507$

| | $f_0(\mathbf{r}-\mathbf{j})$ | | $j_s$ | | | |
|---|---|---|---|---|---|---|
| Star | bcc | fcc | bcc | fcc | hcp | $j$ fcc |
| 2 | 0.196 | 0.180 | 1.732 | 1.782 | 1.782 | 1.782 |
| 3 | 0.122 | 0.045 | 1.847 | 2.028 | 2.028 | 2.520 |
| 4 | 0.023 | 0.012 | 2.390 | 2.633 | 2.576 | 3.086 |
| 5 | 0.0056 | 0.0029 | 2.788 | 2.840 | 2.861 | 3.564 |
| 6 | 0.0041 | 0.0006 | 2.881 | 3.192 | 3.059 | 3.984 |
| 7 | 0.0005 | 0.0001 | 2.986 | 3.300 | 3.30[a] | 4.364 |
| 8 | 0.0002 | 0.0001 | 3.361 | 3.807 | 3.627 | 4.714 |
| 9 | 0.0001 | 0.00004 | 3.599 | 3.860 | 3.83[a] | 5.040 |

[a] Interpolated values.

bcc and for higher energy the fcc. In short we may say that the difference of the bonding and antibonding properties of the eigenstates of the two lattices is determined by their packing.

We may consider $f(\mathbf{r})$ to be an overlap atomic potential (OAP). Then we see that the potential of bcc is smaller than that of fcc. Because OAPs of different lattices have the same mean value $\bar{\bar{V}}$

$$\bar{\bar{V}} \equiv \frac{1}{N} \sum_{\mathbf{j}} \int_{-\infty}^{+\infty} V_0(\mathbf{r}-\mathbf{j}) d\mathbf{r} = \int_{-\infty}^{+\infty} V_0(\mathbf{r}) d\mathbf{r}$$

the extension of the high potential regions in bcc is larger than that of fcc. This shows the difference in the "sperry" character of the lattices [31]. In bcc we have the shorter mean atomic distances but the larger lattice caves.

## 5. The Role of the Potential

We have seen that the kinetic energy differences determine the energy differences between bcc and fcc. Comparing Tables 5 and 6 we see that the potential energy differences behave almost always opposite to those of the energy, but its differences usually are smaller than those of the kinetic energy. The reason for this is that the more the charge density is removed from the surface of the unit cell the more of it stays in the atomic region of deep potential.

We can always describe the potential in a metal with a muffin-tin model as in our Li calculation as long as we are only interested in the energy values. Then the following situation, typical for metals, arises: the total charge density in the atomic region of rapid changing potentials can be considered to be lattice independent. The essential changes

of the distribution probability occur in the interstitial region, where the potential does not change from one lattice to the other. So the potential energy differences between the two lattices almost vanish. In this way we may explain the fact that, especially for metals, band structure energy differences show the same trend for the lattice stability independent of the particular metal.

Other authors have arrived at this conclusion, separately for NFE- and transition metals, in two different ways [9, 12, 13, 15]. Here it is given in a completely new way based on a treatment with localized orbitals. If, by this approach, the same could be proved for transition metals then it would constitute a completely general picture of the metallic bond.

As the symmetry dependence of the differences in the delocalization, respectively the energy of the states, shows we can always expect a change in the lattice stability with a large enough change in VEC. This is caused by the packing effect, which for the same reason favours bcc for the bonding states as it does fcc for the antibonding states.

By the same argument we see that the trend in the lattice stability is not essentially influenced by electron-electron interaction [8, 9, 15].

## 6. The Virial Theorem

For any real compound the virial theorem holds [30].

$$E = \tfrac{1}{2}\bar{V} - \tfrac{3}{2}p\Omega_0$$

$E$ is the total energy, $\bar{V}$ the mean potential energy and $\Omega_0$ the volume of the unit cell. For metals the difference in the total energy of two structures is governed by the difference in the band structure energies [5-9, 12, 13, 15]. Therefore the difference in band structure energy goes with the difference in the potential part of the band structure energy. The $\Omega_0$ dependent term vanishes because the energies of different metal lattices can be compared for equal atomic volume.

If we change the valence electron concentration (VEC), keeping the atomic potential constant, the virial theorem cannot hold any longer. But it holds if we go from one metal to the next (for example in the row Na, Mg, Al), that means, if we change the atomic potential with the VEC. As we know from Sect. 3 the trend in the energy differences is only lattice dependent and therefore holds equally for different metals. So we can understand the lattice stability to a large extent by the influence of the lattice differences on the potential as was done in [31].

Our lithium calculation is not self-consistent and the same potential has been used for core and valence states. In an appropriate self-consistent treatment the virial theorem must hold and we would have transformed kinetic energy into potential energy. In our calculation the energy lower states see a too strongly screened and the higher ones a too less screened potential. Because of the packing effect we expect the mistake in the screening to be largest for bcc. Therefore, compared to fcc, the lower energy states in bcc should be moved into the atomic sphere and the higher energy states into the inter-

stitial regions as is demanded by the virial theorem. In fact, for example an increase of the delocalization can only be accompanied by a decrease of the kinetic energy which has to be compensated by an increase in the potential energy.

## 7. The Role of the Hybridization

In solids, especially in metals, one can define hybridization unambiguously only if one uses for all considered states the same set of basis orbitals as is done in this calculation. It is surprising that this is possible in such a large range of energy.

How this ambiguity arises can simply be seen in the following example. Acting with a projection operator $P_s$ of the total symmetric representation of the inversion point group on the $p$-part of an eigenfunction, we obtain

$$P_s = P_s^+ + P_s^-$$

$$P_s Q_{\mathfrak{k}}\, p^{\nu}_{|\mathfrak{k}|}(\mathfrak{r}) = \frac{2i}{\sqrt{N}} \sum_{\mathfrak{j}} p^{\nu}_{|\mathfrak{k}|}(\mathfrak{r} - \mathfrak{j}) \sin \mathfrak{k}\mathfrak{j} \neq 0$$

in spite of $P_s p^{\nu}_{|\mathfrak{k}|}(\mathfrak{r}) = 0$. We see that we have converted the $p$-symmetry into an $s$-symmetry.

Let us consider a Wannier function [32] defined by

$$a_{\nu}(\mathfrak{r}) \equiv \sum_{\mathfrak{k}}^{\mathrm{BZ}} e^{i\alpha_{\mathfrak{k}}}\, \psi_{\nu\mathfrak{k}}(\mathfrak{r})$$

BZ means the Brillouin zone. If we take in the first case $s$

$$e^{i\alpha_{\mathfrak{k}}} \equiv e^{i\alpha_{-\mathfrak{k}}} \equiv 1$$

and in the second case $p$

$$e^{i\alpha_{\mathfrak{k}}} \equiv -e^{i\alpha_{-\mathfrak{k}}} \equiv 1$$

we obtain

$$a^{(s)}(\mathfrak{r}) = \sum_{\mathfrak{k} \neq -\mathfrak{k}}^{\mathrm{BZ}} (\psi_{\nu,\mathfrak{k}} + \psi_{\nu:-\mathfrak{k}})$$

$$a^{(p)}(\mathfrak{r}) = \sum_{\mathfrak{k} \neq -\mathfrak{k}}^{\mathrm{BZ}} (\psi_{\nu:\mathfrak{k}} - \psi_{\nu:-\mathfrak{k}})$$

$a^{(s)}$ and $a^{(p)}$ are symmetrized Wannier functions [33] of $s$- and $p$-symmetry for which we have the solution of the Schrödinger equation

$$\psi^{(s)}_{\nu:\mathfrak{k}}(\mathfrak{r}) \equiv \frac{1}{\sqrt{N}} \sum_{\mathfrak{j}} e^{i\mathfrak{k}\mathfrak{j}}\, a^{(s)}(\mathfrak{r})$$

$$\psi^{(p)}_{\nu:\mathfrak{k}}(\mathfrak{r}) \equiv \frac{1}{\sqrt{N}} \sum_{\mathfrak{j}} e^{i\mathfrak{k}\mathfrak{j}}\, a^{(p)}(\mathfrak{r})$$

We see that we are able to represent one and the same state by orbitals of completely different symmetry (this holds besides a few states with $k$ in highly symmetric positions). In fact, it is possible to describe all occupied states and therefore the whole chemical bond, for example in the case of lithium, in a very simple way with one such symmetrized Wannier function. This was shown by the author in Ref. [33].

In covalency, hybridization produces directed localized orbitals. In metals, its role is completely different. The hybrids can be oriented in all directions, as is seen by the fact that we have along all three directions 100, 110, and 111 strong $s$-$p$-hybridization. Also no estimate of the energy is possible considering simply the symmetry of the orbitals. The energy difference between bcc and fcc increases with energy. As is seen from Figs. 1, 2, and 3, this holds for the $s$-states $(N_1, L_1)$ as well as for the $p$-states $(N_1', L_1')$. A further reason is that the $s$ and $p$ parts of the functions can be interchanged as was shown above.

But the ratio of the different symmetry contributions to the eigenfunctions may be used as a measure of the energy, as can be seen in Table 11.

Our Ansatz for the eigenfunctions was

$$\psi_{\nu\mathfrak{k}}(\mathfrak{r}) = Q_{\mathfrak{k}}(s^{\nu}_{|\mathfrak{k}|} + ip^{\nu}_{|\mathfrak{k}|})$$

$s$ and $p$ characterize the symmetry parts of the TB orbitals. To arrive at real hybrids we may perform

$$\psi^{+}_{\nu\mathfrak{k}} \equiv \frac{1}{\sqrt{2}}\left[\frac{1}{\sqrt{2}}(\psi_{\nu\mathfrak{k}} + \psi^{*}_{\nu\mathfrak{k}}) + \frac{1}{i\sqrt{2}}(\psi_{\nu\mathfrak{k}} - \psi^{*}_{\nu\mathfrak{k}})\right]$$

$$\psi^{+}_{\nu\mathfrak{k}} = \frac{1}{\sqrt{N}}\sum_{\mathfrak{j}}(\cos \mathfrak{k}\mathfrak{j} \cdot h_{\mathfrak{k}}(\mathfrak{w} - \mathfrak{j}) + \sin \mathfrak{k}\mathfrak{j} \cdot h_{-\mathfrak{k}}(\mathfrak{w} - \mathfrak{j}))$$

$$\psi^{-}_{\nu\mathfrak{k}} \equiv \psi^{+}_{\nu:-\mathfrak{k}}$$

$$h_{\pm\mathfrak{k}}(\mathfrak{r}) \equiv s^{\nu}_{|\mathfrak{k}|}(\mathfrak{r}) \pm p^{\nu}_{|\mathfrak{k}|}(\mathfrak{r})$$

Several orbitals for highly symmetric $k$-points are shown in Figs. 4 and 5.

We know from the considerations of Sect. 2 that the energy values of that structure lie deepest where we have the largest delocalization. By hybridization, this may be achieved in two ways. First by increasing the distribution probability in each state, particularly

Table 11. Ratios of $p$- to $s$-contribution to the square norm of the valence states $\psi_{\nu\mathfrak{k}}$ for the $\mathfrak{k}$ values with the length $a_0^{\mathrm{lat}}/\pi|\mathfrak{k}| = 0.3$ and the directions 100, 110 and 111. $a_0^{\mathrm{lat}}$ is the half lattice constant of bcc, respectively fcc

| | 100 | 110 | 111 |
|---|---|---|---|
| bcc | 0.940 | 0.192 | 0.440 |
| fcc | 1.760 | 0.783 | 0.479 |

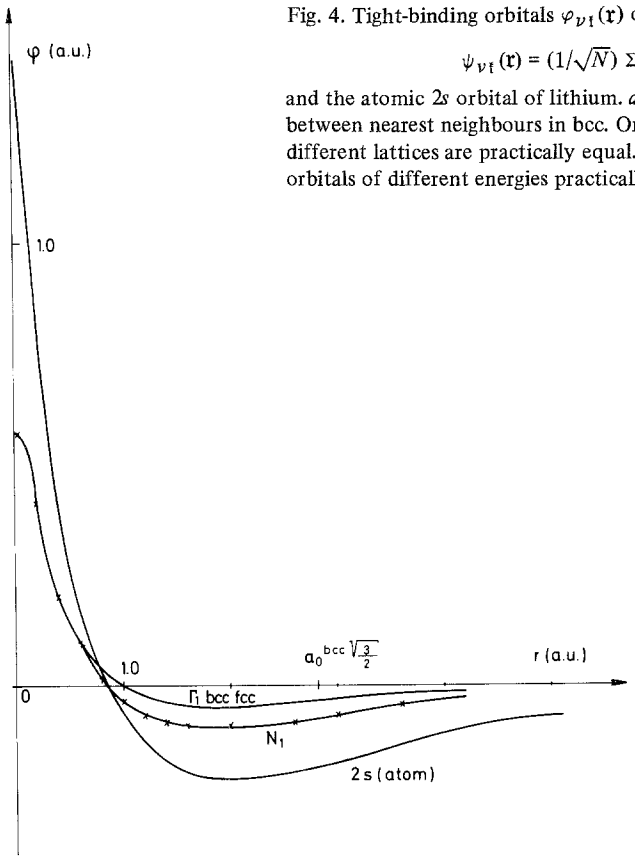


Fig. 4. Tight-binding orbitals $\varphi_{\nu\mathfrak{k}}(\mathfrak{r})$ of several states

$$\psi_{\nu\mathfrak{k}}(\mathfrak{r}) = (1/\sqrt{N})\ \Sigma_{\mathfrak{j}}\ e^{i\mathfrak{k}\mathfrak{j}}\ \varphi_{\nu_{\mathfrak{k}}}(\mathfrak{r} - \mathfrak{j})$$

and the atomic $2s$ orbital of lithium. $a_0^{bcc}\sqrt{3/2}$ is the half distance between nearest neighbours in bcc. Orbitals of comparable $\nu_{\mathfrak{k}}$ but different lattices are practically equal. Also, in the atomic region orbitals of different energies practically do not differ

between neighbouring atoms, and secondly by increasing the number of states for which this happens. Both trends try to distribute the charge density spherically around the atomic centres and this may occur at different distances from the centre in different lattices. Also, any resemblance of the lattice differences in the charge distribution with that of directed bonds may be understood as a superposition of different spherically distributed charges.

The first case may happen if, for example, an antibonding $s$-function mixes with a bonding $p$-function. From Table 5 we see that we have for fcc the smaller energy separation between the $s$- and $p$-bands. In addition, as the distances in the 100 direction are very different we see, particularly from comparison of the energies in this direction, that fcc favours the hybridization. This holds more as the energy in the $s$-band increases and it is not restricted to 100, as we see from Table 11. So, with increasing VEC, hybridization favours fcc against bcc.

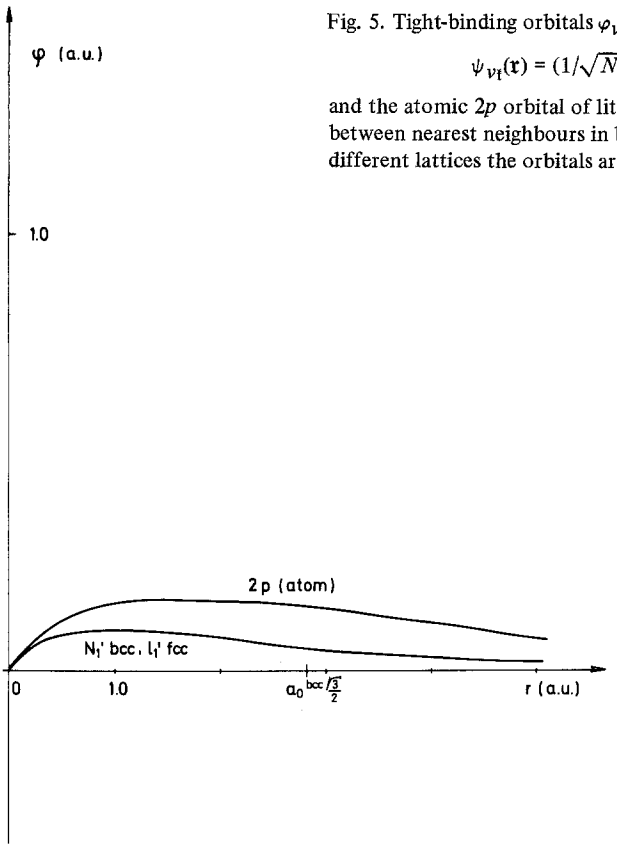


Fig. 5. Tight-binding orbitals $\varphi_{\nu\mathfrak{k}}(\mathfrak{r})$ of two states

$$\psi_{\nu\mathfrak{k}}(\mathfrak{r}) = (1/\sqrt{N})\,\Sigma_{\mathfrak{j}}\, e^{i\mathfrak{k}\mathfrak{j}}\varphi_{\nu\mathfrak{k}}(\mathfrak{r}-\mathfrak{j})$$

and the atomic $2p$ orbital of lithium. $a_0^{\mathrm{bcc}}\sqrt{3/2}$ is the half distance between nearest neighbours in bcc. In spite of belonging to two different lattices the orbitals are practically equal

## 8. A Glance at the Transition Metals

It should be noticed that this work never makes use of the facts that are only characteristic of the NFE-metals. The TB-method and the essence of the considerations presented could also apply to transition metals. We have already seen that in principle it is possible to describe a *d*-band with tight-binding orbitals of any symmetry we wish (with the restriction mentioned in the foregoing section). For the tight-binding method therefore the *d*-symmetry makes no principle difference to a treatment with *s*- or *p*-orbitals. Further on, the packing effect is completely geometrical and does not depend on the range of interaction between the atoms. Therefore, we would expect that for transition metals the stability sequence with increasing VEC is bcc–fcc.

Concerning the hybridization, Altmann, Coulson and Hume-Rothery [34, 35] gave an explanation based on directed hybrids. For example, they give a stronger *s*-*p*-mixing with the *d*-states for fcc than for bcc. This seems to agree with the present work. However, the hybridization is interpreted completely different here and we would also have to consider the hybrids of those resonance structures which the above-mentioned authors assumed did not contribute to the determination of the structure and were, therefore, neglected.

## 9. Summary

This work presents the first comparison of metal lattices using a TB calculation. The essential characteristics are that pure Gaussians have been used to represent the basis functions and a model potential was used which produces the band structure energy differences only by differences in the geometry of the bcc and fcc lattices.

The band structure energy difference is determined in this non-self-consistent calculation by the kinetic band structure energy difference. This depends on the dissimilarity in the delocalization of the distribution probability. The more delocalized states have the lowest energies.

This difference in turn is determined by the variance in the geometrical packing of the lattices which is characterized by the mean length of the vectors of the lattice stars which are smaller for bcc than for fcc. This distribution probability of the more bonding states of bcc is caused to be more delocalized than in fcc. The reverse holds for the antibonding states. Comparing bcc with fcc, their increase in energy is for the same reason as the decrease of the energy of the bonding states.

The generality of these considerations is especially shown by an empty lattice test, in which the trend in the band structure energy difference is the same as for the calculation with non-vanishing potential. It shows that for metals, the band structure energy differences are really determined by the packing effect, that their trend is the same for all NFE-metals and that we always have to expect a change in the lattice stability if VEC is sufficiently changed.

The virial theorem demands that the mean potential band structure energy varies as the band structure energy differences. This would happen if we were to make a self-consistent calculation.

The hybridization plays a completely different role from that in a covalent solid. For metals, it favours that structure which has the most delocalized charge density. Because of the generality of the considerations given, they should also hold for transition metals.

*Acknowledgement.* I have to thank Prof. H. Bilz for his kind support. It is a great pleasure for me to thank Prof. S. Rabii for many valuable discussions.

## References

1. Lafon, E. E., Lin, C. C.: Phys. Rev. **152**, 579 (1966)
2. Chaney, R. C., Tung, T. K., Lin, C. C., Lafon, E. E.: J. Chem. Phys. **52**, 361 (1970)
3. Chaney, R. C., Lin, C. C., Lafon, E. E.: Phys. Rev. **B3**, 549 (1971)
4. Krebs, H.: Grundzüge der anorganischen Kristallchemie. Stuttgart: Ferdinand Enke Verlag 1968
5. Harrison, W. A.: Pseudopotentials in the theory of metals. New York: W. A. Benjamin 1966
6. Hafner, J., Nowotny, H.: Phys. Stat. Sol. (b) **51**, 107 (1972)
7. Hafner, J.: Phys. Stat. Sol. (b) **56**, 579 (1973)
8. Hafner, J.: Phys. Stat. Sol. (b) **57**, 101 (1973)
9. Heine, V., Weaire, D.: Solid State Phys. **24**, 249 (1970)
10. Hubbard, J.: Proc. Phys. Soc. **92**, 921 (1967)
11. Hubbard, J., Dalton, N. W.: J. Phys. C. **1**, 1637 (1968)

12. Dalton, N. W., Deegan, R. A.: J. Phys. C. 2, 2369 (1969)
13. Deegan, R. A.: J. Phys. C. 1, 763 (1968)
14. Pettifor, D. G.: J. Phys. C. 2, 1051 (1969)
15. Pettifor, D. G. in: Metallurgical chemistry, O. Kubaschewski Ed.: London: National Physical Laboratory, 1972
16. Averill, F. W.: Phys. Rev. **B6**, 3637 (1972)
17. Rudge, W. E.: Phys. Rev. **181**, 1024 (1969)
18. Ellis, D. E., Painter, G. S.: Phys. Rev. **B2**, 2887 (1970)
19. Chaney, R. C., Lafon, E. E., Lin, C. C.: Phys. Rev. **B4**, 2734 (1971)
20. Kumar, L., Monkhorst, H. J., Harris, F. E.: Phys. Rev. **B9**, 4084 (1974)
21. Averill, F. W.: Phys. Rev. **B4**, 3315 (1971)
22. Seitz, F.: Phys. Rev. **47**, 400 (1975)
23. Whitten, J. L.: J. Chem. Phys. **44**, 359 (1966)
24. Fock, V., Petrashen, M. J.: Physik. Z. Sowjetunion **8**, 547 (1935)
25. Kohn, W., Rostoker, N.: Phys. Rev. **94**, 1111 (1974)
26. Schlosser, H., Marcus, P. M.: Phys. Rev. **131**, 2529 (1963)
27. Ham, F. S.: I, Phys. Rev. **128**, 82 (1962); II, Phys. Rev. **128**, 2524 (1962)
28. Glasser, M. L., Callaway, J.: Phys. Rev. **109**, 1541 (1958)
29. Callaway, J.: Phys. Rev. **124**, 1824 (1961)
30. Slater, J. C.: Quantum theory of molecules and solids. New York: McGraw-Hill 1966
31. Reiser, B.: Theoret. Chim. Acta (Berl.) to be published
32. Wannier, G. H.: Phys. Rev. **52**, 191 (1937)
33. Reiser, B.: Phys. Rev. **B13**, 1587 (1976)
34. Altmann, S. L., Coulson, C. A., Hume-Rothery, W.: Proc. Roy. Soc. **A240**, 145 (1957)
35. Home-Rothery, W.: Atomic theory for students of metallurgy. London: The Institute of Metals, 1962

*Received December 17, 1975/May 17, 1976*